IV. Semester Report

Németh Patrik (npatrik213@protonmail.com)

Astronomy and Space Physics PhD program

Supervisor: Fernando Cruz-Sáenz de Miera

Title of the thesis: Near-infrared spectroscopy of eruptive young stars: new discoveries and long term follow-up observations

2024.05.31.

Introduction:

Protostars form in the densest molecular cloud cores. Due to the non-zero angular momentum of the initial cloud, matter forms a disk around it. In this orbiting disk, the material slowly spirals inwards and accretes onto the surface of the star. Accretion hits up the disc, causing it to be bright, and thus it causes the disc to be significant contributor to the bolometric luminosity of the young stellar objects (YSO). Therefore, it is expected any changes in these mass accretion rates are reflected as changes in the brightness of the young stars. One group of YSOs are young eruptive stars. These objects show large outbursts in visible and near-infrared light ($\Delta mag > 1$). The luminosities suggest an increase in the mass accretion rate.

My project will be to identify new eruptive young stars. To do this, I use measurements from the Gaia space telescope or the Zwicky Transient Facility, which have an alerts program that reports if there are sudden changes in the photometry of a star. Afterwards, I will examine whether they are in a star forming region by analyzing their coordinates and distances and, finally, will compile their spectral energy distribution to verify that they a young stellar object. After these steps, I will be confident that these sources are good eruptive young star candidates, and prepare follow-up optical and near-infrared observations to obtain their spectra. For these spectroscopic observations, some of the facilities that I will request time for are the Very Large Telescope and the Nordic Optical Telescope. I will identify the spectral lines which are typical indicators of mass accretion rate (e.g. Hα, Paβ, Brγ), search for indications of a P-Cygni line profile, which is common in eruptive young star, and estimate the mass accretion rate from the accretion luminosity. I will follow up by analyzing the CO band heads (>2.29 μm), and of other lines (e.g. Fe I, Na I and Ca I) to estimate the geometry of the circumstellar disk. Finally, I will search for jets, using different forbidden metallic and H_2 lines.

Description of research work carried out during the four semester:

During this semester I spend most of my time to finish the paper about Gaia20dsk YSO candidate. Currently I await feedback from my peers, which suggestions can enhance the quality of my research and my papaer. Additionally, I have made necessary revisions to certain dates based on newly available information.

In summarizing the results of my research spanning both this semester and the previous ones, I have arrived at the following conclusions.

Location of the star:

Gaia20dsk is situated at a substantial distance of approximately 2542 parsecs. Additionally, this source appears faint, with a magnitude of about 19 in the G band during its quiescent stage. Considering the errors on the distance and the proper motion of this source, it can be a part of a

well-known star-forming region, namely NGC6334. Firstly, its coordinates align with this region in the sky. Secondly, the proper motion of the source indicates the same direction as other members of the group. Generally, it shares a similar μ_{ra} to other parts of the group, with only a slight difference in μ_{dec} , which can be attributed to various effects. For instance, our source may not be a close member of this cluster. Finally, considering the errors in the distance of Gaia20dsk, it could fall within the distance range of other parts of the cluster.

Light curve:

In Fig. 1, the light curve of Gaia20dsk illustrates the changes in Gaia G magnitude over time. In this figure, the blue circles represent the Gaia G magnitude, with filled circles indicating alert times and their corresponding magnitude values. The dashed line signifies the time when the X-SHOOTER spectrum was taken. As illustrated in the figure, the brightening began in March 2020 and continued for approximately half a year before fading. The average magnitude during the brightening was around 19, increasing to around 17.2 afterward. This change amounted to approximately 1.9 magnitudes and spanned a year. Based on the most recent data available until October 2023, it seems that the source, which previously exhibited a fading trend, has started to brighten again, reaching a new peak at about 17.4 mag. This brightening event is not attributed to periodic occurrences, as there has been no discernible change in the light curve during the five years leading up to the first peak.

The swift increase in brightness over a short period aligns with observations of many EXor-type stars (Jurdana-Šepić et al. 2018b[a]). Additionally, the recurring nature of these events can be characteristic of this class (Cruz-Sáenz de Miera et al. 2022[b]). The magnitude of the initial 1.9 brightening and the duration of the first event further support the EXor hypothesis, which show typical brightening of V = 1-4 mag over several months to years (Fischer et al. 2023[c]).

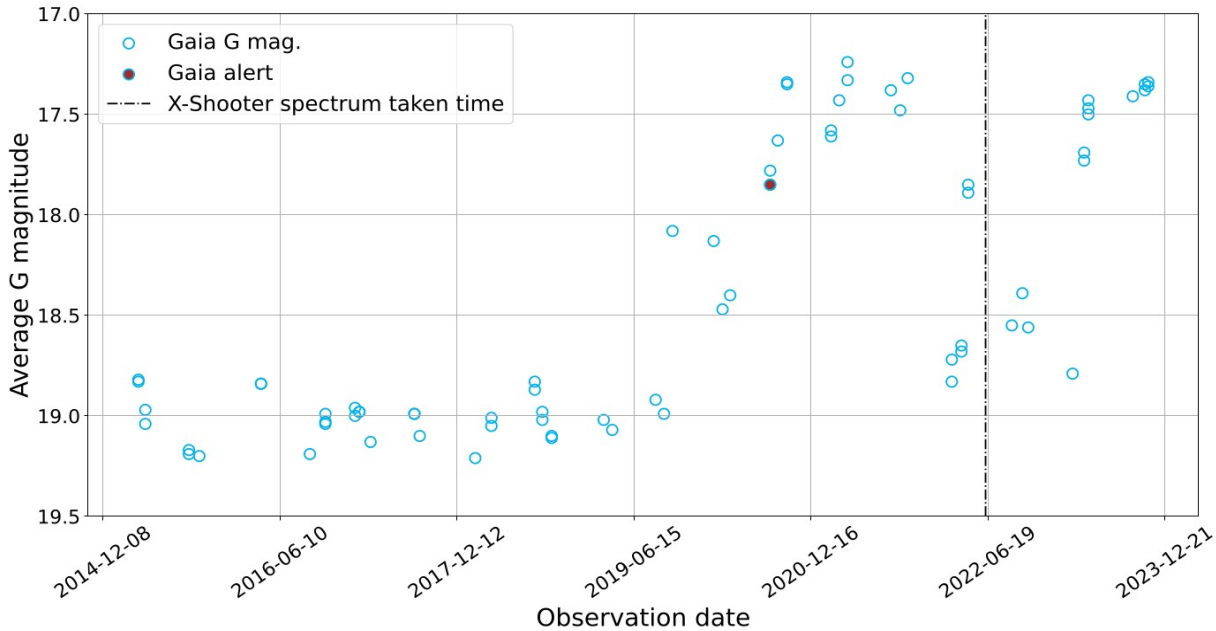

Figure 1: Gaia20dsk light curve. The unfilled circles represent the Gaia magnitude measurements of the stars taken since the end of 2014. The dashed line indicate the time when the spectrum of the Gaia20dsk was captured using X-Shooter while the red filled circle indicate the time of Gaia alerts.

Spectral energy distribution (SED):

The SED of the source was constructed using archival data from various instruments, each represented by different colors in the Fig. 2. Photometric measurements were obtained from the VO

SED Analyzer (VOSA) services database (Bayo et al. 2008[d]), utilizing data from Gaia, 2MASS, WISE, and Spitzer. The SED, which is depicted in Fig. 2. is not corrected for extinction. The SED exhibited a shallow slope towards longer wavelengths, deviating from a typical single temperature black body shape. This deviation suggests an infrared excess, possibly originating from the accretion disc surrounding the star (Mendoza V. 1968[e]). Notably, the SED peaked in the Near-Infrared, with noticeable differences between Gaia and 2MASS data points. Additionally, the X-SHOTTER obtained spectrum displayed noise in the UV and VIS range, hinting at the possibility that the star is still enveloped, hindering the detection of energy from shorter wavelengths.

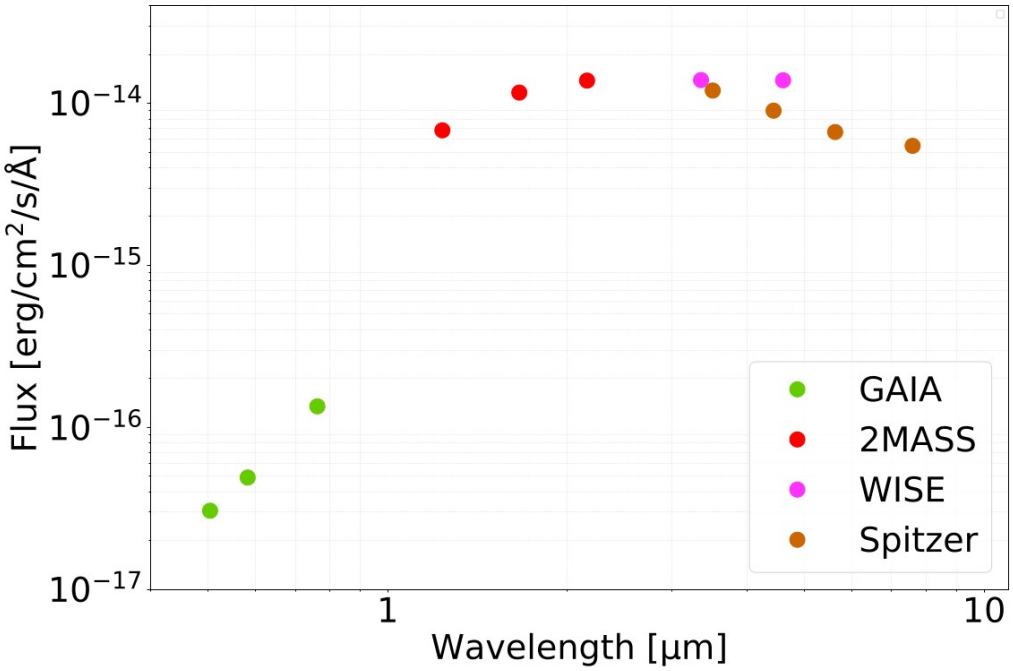

Figure 2: Gaia20dsk Spectral Energy Distribution. The data points, sourced from the VO SED Analyzer database, represent photometric measurements from various surveys. Different colored dots denote different surveys: green for Gaia (Bp, G, Rp) from Gaia DR3, red for 2MASS (J, H, K), purple for WISE (W1, W2), and brown for Spitzer (I1, I2, I3, I4). The points are not corrected for extinction.

Spectrum:

The spectrum displayed medium-resolution spectra covering approximately the range from 4600Å to 24000Å. It show increasing flux density towards longer wavelengths. The parts with significant noise below approximately 7500Å and sections heavily affected by telluric lines was removed, as illustrated in Fig 3. Besides the identified magnetic accretion tracer lines there was detected the HeI 10830 Å, exhibiting a broad absorption component believed to be formed by a stellar wind (Erkal et al. 2022[f]).

I identified 9 lines which are considered as accretion tracer influenced by magnetic field lines (Alcalá et al. 2017[g]). After the photosphere subtraction (next section), all of the line have a single peak shape. In the case of Brγ and CaII, they showed a double peak shape before the photosphere subtraction. Based on the photospheric data, I can conclude that the absorption effect was caused by the photosphere.

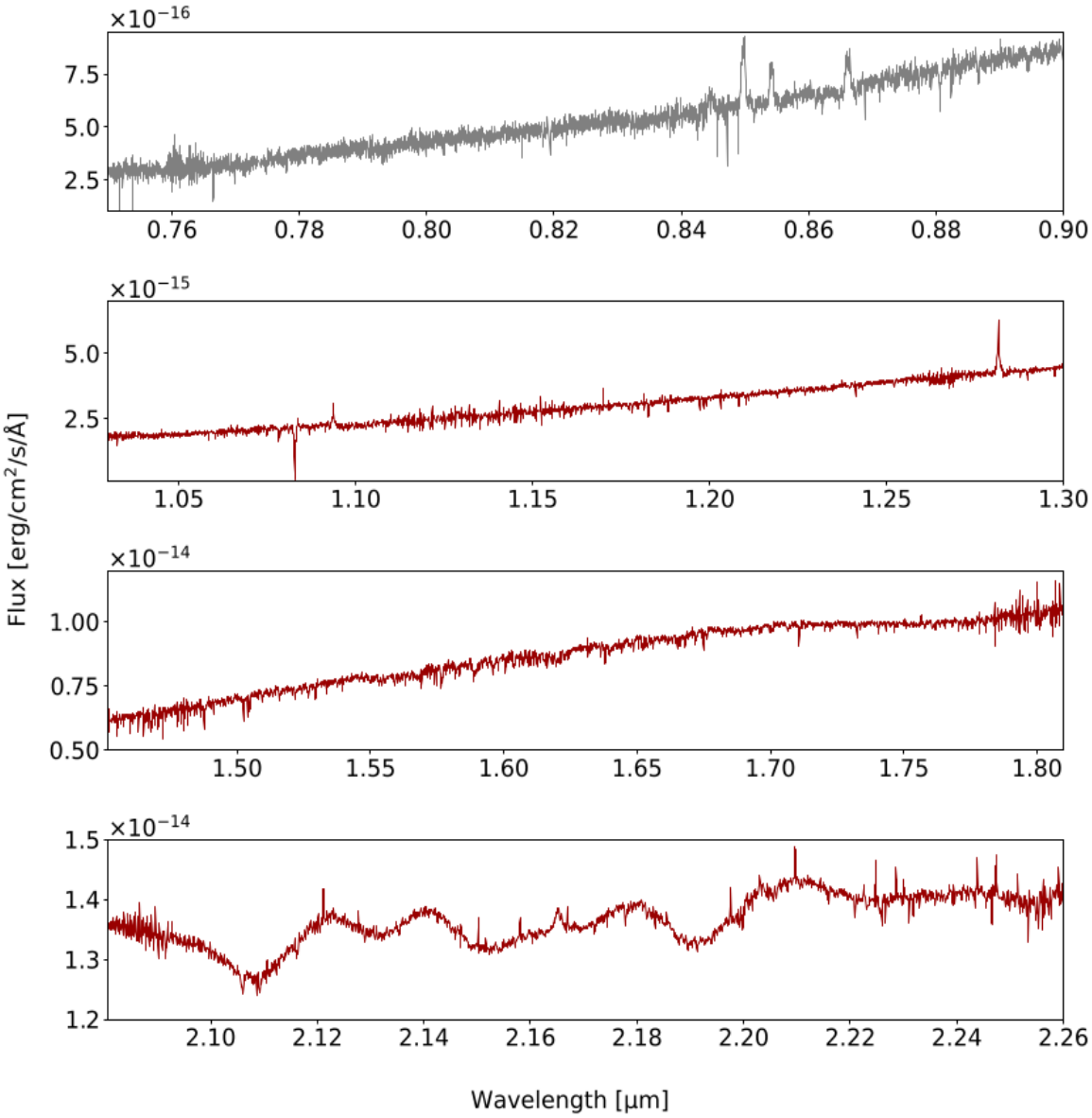

Figure 3: Spectrum of Gaia20dsk taken by X-SHOOTER on June 12, 2022. The optical part is represented by gray, while the infrared range with red color. The spectrum is not corrected for extinction. The noisy part below, 7500 Å were removed. The spectrum mostly contains emission lines, which of some considered as tracer of magnetic accretion process. The spectrum itself shows increasing flux density in a direction of longer wavelength.

Mitigation of veiling:

I attempted to mitigate the influence of the photospheric absorption features in the Gaia20dsk spectrum, aiming to reveal new insights from the emission lines. This approach was based on the ’The X-shooter Spectral Library’3 (XSL; Verro et al. 2022), which contains 830 stellar spectra for 683 stars observed with the X-SHOOTER spectrograph. During the process, I compared the spectra of the stars (referred to as templates) from the aforementioned database to the Gaia20dsk spectrum. For this I constructed a python code, which autonomously implement the most of the steps.

The steps explanation rely on the Figure 4. At the beginning I had chosen a spectral range in the Gaia20dsk spectrum, which contain only absorption lines within a few 10 Angstrom range, and where the spectrum was not too noisy. This approach facilitated automated continuum identification in most cases while providing numerous absorption lines for template comparison. The first range where I found many absorption features with good S/N was between 8770Å and 8840Å. The code first read the Gaia20dsk spectrum, determined the continuum level, and fitted it using the fit_continuum python routine from the specutils.fitting.continuum module. Subsequently, the flux density was normalized using the fitted continuum level. This spectrum is signified by blue on the top panel of Fig. 4. In the template comparison step, the code iteratively read in template stars, filtering them based on specific properties (similar to TTauri) such as spectral type (F, G, or K), metallicity within the range of [-0.5, 0.5], and surface gravity (log(g)) within [3, 4.5]. Each template spectrum meeting these criteria underwent continuum fitting and flux density normalization. Finally, I constructed a function which "corrects" the veiling. Virtually we scaled the normalized template flux density iteratively until achieving the lowest chi-square value between the template and the Gaia20dsk spectrum (see the spectrum with magenta on the top panel of Fig. 4). Then, utilizing these veiled normalized template and the Gaia20dsk spectrum, the code performed another 2 test to assess their resemblance.

Additionally, to validate the results, we visually inspected the fits to ensure no potential good fits were overlooked. While some challenging cases arose, such as rapidly changing continuum shapes or broad blended absorption features, these instances did not significantly impact the final results of our code. As the code is finished, and we inspected the fits by eye, I took the 6 sources with the best chi2 value. I plotted them with the Gaia20sk spectrum in the same range, where the identified mass accretion tracer lines are located. For this, you can see an example on the middle plot of Fig. 4, in the case of one of the Calcium triplet (CaII)lines. I applied a veiling correction by excluding the portions of the two spectra containing emission features (signified by orange part on the plot) and utilizing the adjacent spectral range for correction (denoted by magenta part). Upon completion all of the process, HD 188262 emerged as the best-matched spectrum. Finding the final star, I subtracted the two normalized spectrum from each other (which are shown in the middle panel in Fig 4), and then I scaled it back with the level of continuum of Gaia20dsk. The resulted plot is depicted on the bottom plot in Fig. 4. As for the HD 188262; it is a bright giant with spectral type of G8II. The logg is 3.2 cm/s2 , while metallicity is 0.22. I refrain from classify some basic information based on the resulted star, because on one hand our star is probably not a giant, and on the other hand during the comparison there was some absorption feature which was not fitted well, despite the veiling correction.

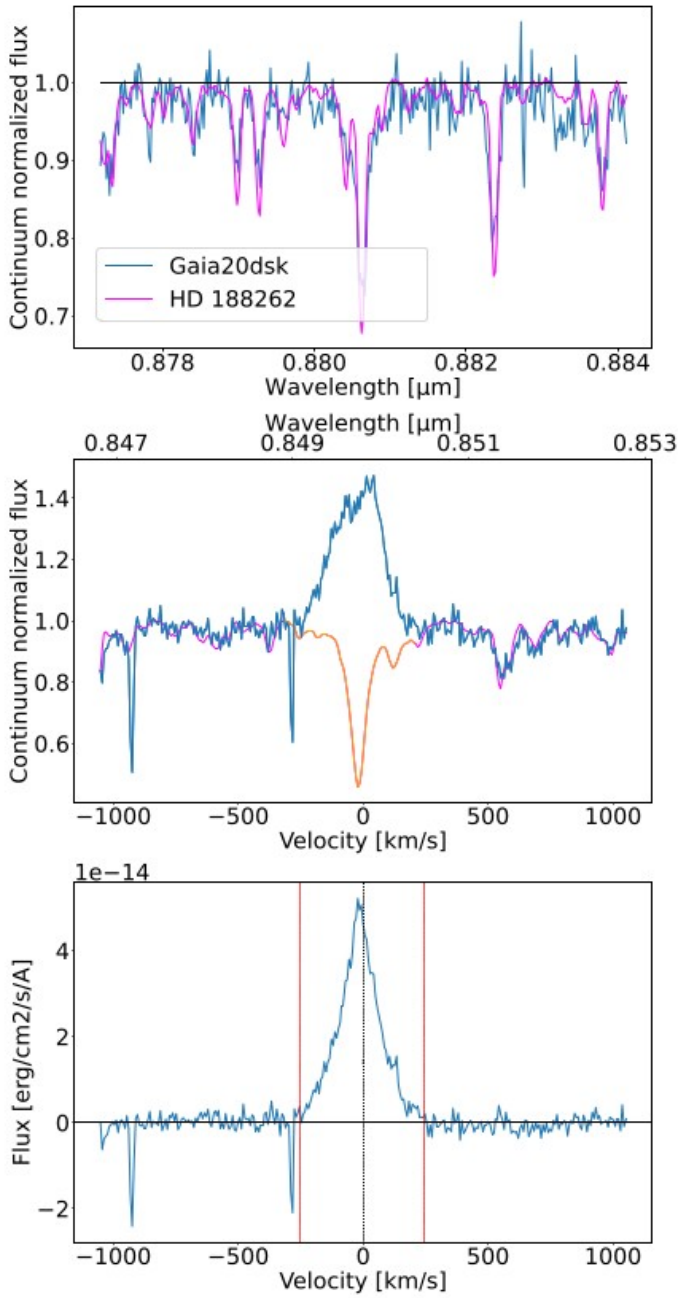

Figure 4: Top panel: displays photospheric absorptions from Gaia20dsk, depicted in blue, and HD188262, represented in magenta. The middle panel show cases one of the accretion tracing emission lines before correction with the best-fit photosphere. The colors indicate the same sources as in the top panel. The orange region in the middle plot denotes the range that was removed during the veiling correction. Bottom panel: shows the photosphere subtracted accretion-tracing line. In the bottom panel, the red lines indicate the portion within which the flux of the line was calculated. In both the middle and bottom panels, the absorption features observed at approximately ~-300 km/s and ~-900 km/s are associated to instrumental effect.

Shape of spectral lines:

After the photosphere subtraction, all of the line have a single peak shape. In the case of Brγ and CaII, they showed a double peak shape before the photosphere subtraction. Based on the photospheric data, we can conclude that the absorption effect was caused by the photosphere.

All of the identified mass accretion tracer lines show at least a slight blue shift, except for the CaT, which are right at their rest wavelength approximately. The two lines which show the strongest shift are: Brγ and Paβ with approximately -100 - -110 km/s respectively. This huge blue shift can indicate that these lines may trace also outflow (Whelan et al. 2004[h]). In addition to this, Brγ is a very broad (about 400 km/s in width). This can also support the wind origin (Bik et al. 2006[i]). On the other hand Paβ also posses a broad component, which has roughly the same width as of Brγ.

Additionally, Paβ has narrow component on the top of the broad. This indicates that the line have different generation region, or it is generated under different physical conditions. In the longward vicinity of the Brγ I found a peak in the spectrum, what we can't conclude as a frequent, known line. The Pa9 shows some absorption feature on the right wing. The Hα shows a single peak shape. The trunk of the line is much narrower, 200 km/s; half of the width compared to other lines. And it is mentionable, that the line shows some very shallow, elongated, weak emission features on its left and its right wing. As for the lines from a Paschen series, all of the line have stronger flux density on their bluer wing compared to their red wing. This broad blue emission line wing signatures can be interpreted as indication of outflows (Panizo-Espinar et al. 2022[j]).

The spectrum predominantly exhibits emission lines dominated by HI recombination, typical of EXor spectra. (Lorenzetti et al. 2012[k]). Notably, nine of the identified lines serve as tracers for the accretion process driven by magnetic field lines, characteristic of low-mass young stellar objects (Hartmann et al. 1994[l]). Supporting the magnetic accretion theory, most of the accretion tracer lines display broad line shapes exceeding 200-300 km/s, suggesting broadening mechanisms caused by infalling material reaching free-fall velocities towards the star's surface (Hartmann et al. 2016[m]). Additionally, many lines exhibit a narrow component superimposed on the broad one, indicating different origins with distinct physical effects. Brγ and Paβ display blue-shifted peaks exceeding 100 km/s, potentially indicative of partial generation in wind or outflow processes.

Mass accretion rate:

The identified 9 accretion tracer lines serve as asset to determine the mass accretion rate of the star, assuming accretion driven by magnetic field lines. I followed the method described in the Alcalá et al. (2017) paper, illustrating the process with an example: Hα. The Fig. 5 represents the extinction corrected, continuum and photosphere subtracted flux density of the Hα. The dotted line represents the rest wavelength of the line, while the orange lines indicate the boundaries within I calculated the line flux. Heliocentric velocity correction was applied using the heliocentric_corr Python routine from the Heliocentric_correction module. The line_flux Python routine from the specutils.analysis module was used to determine the line flux. The mass accretion then was calculated based on forementioned paper.

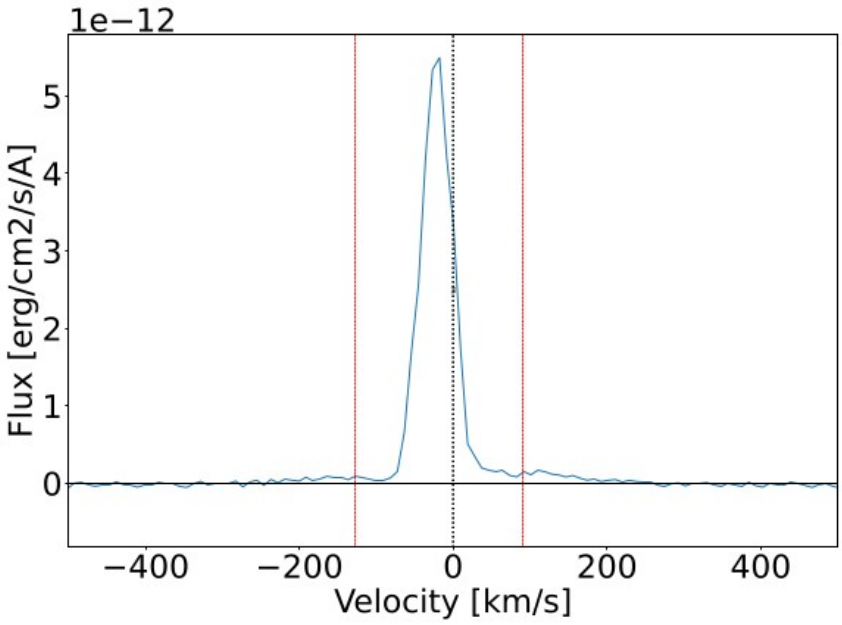

Figure 5: Flux density of the continuum subtracted H*α* line as a function of wavelength. One of the identified accretion tracer line. The dotted line signify the rest wavelength of the line. The red line delimit the range within the flux of the line is calculated.

In Fig. 6, the results of the mass accretion rate computation are presented. The x-axis lists the lines as follows: Hα, lines from a Paschen series (where y = 9, δ, γ, β), and Brγ . The numbers after the letters indicate the upper energy level of the transition in the series. CaII represents the Calcium II triplets. The overall trend is around $2x10^7$ $M_\odot$/year. This value aligns with the typical mass accretion rates for EXor: $\dot{M}$ = 10^7 $M_\odot$/year - 10^6 $M_\odot$/year (Stock et al. 2020[n]). The Hα is out of tendency upward. It can explained with the fact that this line do not trace only the accretion, but instead other effects which contribute its strengths (Alcalá et al. 2014[o]). On the other hand Pa9 not as extent as Hα, but as well stick out of tendency. It may can accounted for by that this line show some absorption feature on its red side, which reduces its flux. It's important to note that the spectrum was obtained at the end of the brightening stage. Therefore, I can infer that the Macc may have been stronger at its peak.

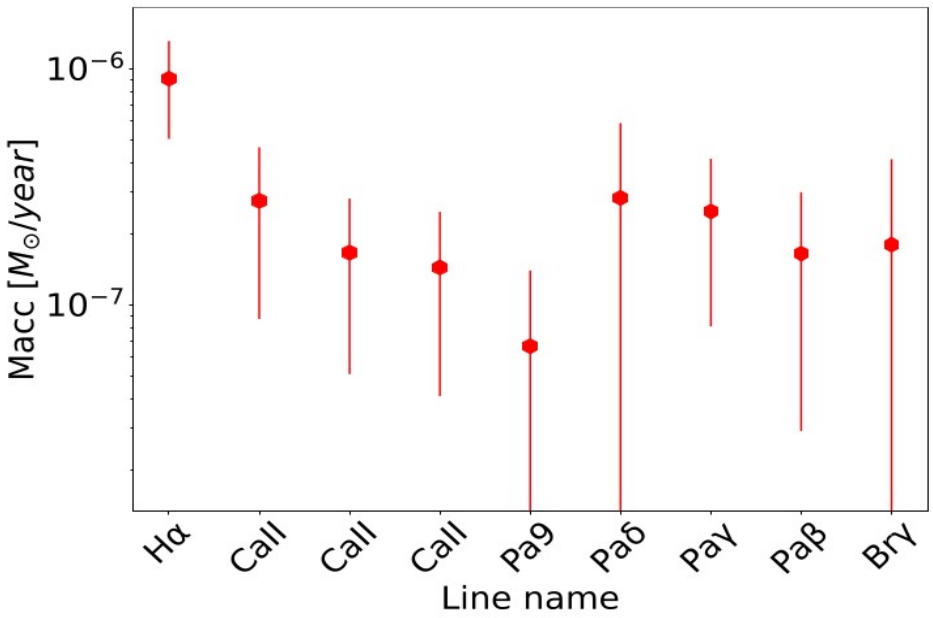

Figure 6: Gaia20sdk mass accretion rate. The red hexagons represent the mass accretion rates from each identified line. On the x-axis the lines name are the follows: Hα line is part of the Balmer series, Pay lines are part of the Paschen series (where y = 9, δ, γ, β), and the Brγ is part of the Bracket series. The numbers after the letters associated to the upper energy level of the transmission in the series. The three CaII are the CalciumII triplets.

Classification:

Since the classification method proposed by Lada (1987) based on the SED, numerous alternative methods have emerged, particularly those linked to infrared photometry. One such approach involves employing a color-color diagram, utilizing data from 2MASS and WISE measurements. In the case of the Gaia20dsk source, I applied a color-color diagram method, based on Fig. 6 in the work of Koenig & Leisawitz (2014)[p]. Utilizing 2MASS J and H photometry along with WISE W1 and W2 photometry, I derived the following color indices: J-H: 1.685 | W1-W2: 1.266. Placing these values on the aforementioned figure, this analysis suggests that the star could be classified as a Class I object.

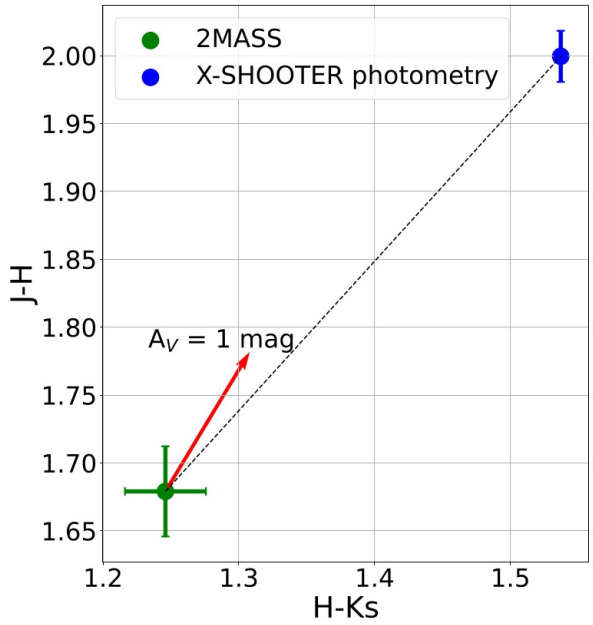

Figure 7: Measured and synthetic 2MASS color-color diagram. The green dots correspond to the measured 2MASS data from 1998. The blue dots represent synthetic photometry calculated from the X-SHOOTER spectrum. The red arrow direction and size signifies the cause of 1 mag extinction. The difference between the dashed line connects the two points to each other and the extinction vector; suggests that observed color changes are attributable to real physical effects, not directly caused by changes in extinction.

Studies in current semester:

FIZ/5/015 Infrred Astronomy I.
FIZ/5/032 The physics of interstellar matter II.

Teaching activity in current semester:

ELTE cseszlgyk3g17ga – Csillagászati észlelési gyakorlatok 3.; 2 lessons per week

Activities in scientific associations:

I attend the meetings of ‘Gaia alerts’ groups at Konkoly observatory.
I work on ongoing research on sources detected in the Gaia Photometric Science Alerts system under the guidance of Dr. Zsófia Nagy.

References:

[a] Jurdana-Šepić, R., Munari, U., Antoniucci, S., Giannini, T., & Lorenzetti, D. 2018, A&A, 614, A9
[b] Cruz-Sáenz de Miera, F., Kóspál, Á., Ábrahám, P., et al. 2022, ApJ, 927, 125
[c] Fischer, W. J., Hillenbrand, L. A., Herczeg, G. J., et al. 2023A, 534, 355
[d] Bayo, A., Rodrigo, C., Barrado Y Navascués, D., et al. 2008, A&A, 492, 277
[e] Mendoza V., E. E. 1968, ApJ, 151, 977
[f] Erkal, J., Manara, C. F., Schneider, P. C., et al. 2022, A&A, 666, A188
[g] Alcalá, J. M., Manara, C. F., Natta, A., et al. 2017, A&A, 600, A20
[h] Whelan, E. T., Ray, T. P., & Davis, C. J. 2004, A&A, 417, 247
[i] Bik, A., Kaper, L., & Waters, L. B. F. M. 2006, A&A, 455, 561

[j] Panizo-Espinar, G., Armas Padilla, M., Muñoz-Darias, T., et al. 2022, A&A, 664, A100
[k] Lorenzetti, D., Antoniucci, S., Giannini, T., et al. 2012, ApJ, 749, 188
[l] Hartmann, L., Hewett, R., & Calvet, N. 1994, ApJ, 426, 669
[m] Hartmann, L., Herczeg, G., & Calvet, N. 2016, ARA&A, 54, 135
[n] Stock, C., Caratti o Garatti, A., McGinnis, P., et al. 2020, A&A, 643, A181
[o] Alcalá, J. M., Natta, A., Manara, C. F., et al. 2014, A&A, 561, A2
[p] Koenig, X. P. & Leisawitz, D. T. 2014, ApJ, 791, 131